Available online at www.sciencedirect.com
ScienceDirect
Geochimica et Cosmochimica Acta 71 (2007) 4592–4608
Geochimica et Cosmochimica Acta
www.elsevier.com/locate/gca

Geo- and cosmochemistry of the twin elements yttrium and holmium

Andreas Pack [a,b,*], Sara S. Russell [c], J. Michael G. Shelley [d], Mark van Zuilen [a,e]

[a] CNRS Centre de Récherches Pétrographiques et Géochimiques, 15 rue Notre Dame des Pauvres, F-54501 Vandoeuvre-lès-Nancy, France
[b] Institut für Mineralogie, Universität Hannover, Callinstrasse 3, D-30167 Hannover, Germany
[c] Department of Mineralogy, The Natural History Museum, Cromwell Road, London SW7 5BD, UK
[d] Research School of Earth Sciences, The Australian National University, Canberra, ACT 0200, Australia
[e] Institut de Physique du Globe de Paris, Tour 14, 5e étage, Aile 14-15, Case 89, 4 Place Jussieu, F-75252 Paris, France

Received 11 April 2006; accepted in revised form 12 July 2007; available online 2 August 2007

Abstract

We have analyzed the Y/Ho-ratios in bulk chondrites, chondrules and four Ca- and Al-rich inclusions (CAIs) from carbonaceous and unequilibrated ordinary and enstatite chondrites (EC) by laser ablation inductively coupled mass spectrometry (LA-ICPMS). We demonstrate that bulk rock sample preparation by containerless melting is a suitable method for preparation of bulk rock samples for high-precision LA-ICPMS. Bulk chondrites have variable Y/Ho-ratios. Carbonaceous chondrites (CI1, CM2, CV3, and CK4) have a common Y/Ho-ratio (25.94 ± 0.08, 2σ) that is regarded as the solar system Y/Ho-ratio. The Y/Ho-ratio increases from carbonaceous, through ordinary (LL, L, H) to enstatite chondrites (EL6), which show the highest Y/Ho-ratio of 27.25. We discuss the result with respect to the origin of fractionation of Re and Os between chondrite groups. Within analytical error, Y and Ho show a good correlation in OC and CV3 chondrules and define an Y/Ho-ratio of 26.22 ± 0.40 (2σ). Y/Ho-fractionation in Ca- and Al-rich inclusions is related to differences in volatility. The bulk silicate Earth is suggested to have a solar Y/Ho-ratio and links the Earth with carbonaceous chondrites. Y/Ho variations in primitive and differentiated terrestrial igneous rocks are discussed in framework of incompatibility of Y and Ho during partial melting. Applicability of Y/Ho as tracer for or against a sedimentary origin of the putative host rock of the Earth's oldest traces of life from the island of Akilia is briefly discussed.

1. INTRODUCTION

1.1. Origin of Y and Ho

The solar system abundances of elements with $Z > \sim 56$ are a function of their stellar production-rates (until 4.6 Ga ago). Elements heavier than Fe and Ni form by two different neutron caption processes (*n*-capture process). The *r*-process occurs during type-II supernovae and requires high neutron flux. It is a primordial process and does not requires preexisting *n*-capture elements, i.e., it operated early in the galactic evolution when metallicity was low. Spectral analyses of ultra metal-poor (i.e., very old) galactic halo stars show that they contain mainly *r*-process nuclides (Burris et al., 2000).

The *s*-process operates at lower neutron fluxes during the double shell-burning phase of low- to intermediate mass stars (1–7 $M_{\odot}$). It is a non-primordial process and requires preexistence of *n*-capture elements. Contribution from the *s*-process became important only later in the evolution of the galaxy at metallicities [Fe/H] > 2.7.

Y and Ho are both mono-isotopic. According to calculations by Burris et al. (2000), solar system Y contains ~28% *r*- and ~72% *s*-process component. This ratio reflects

* Corresponding author. Address: Arbeitsgruppe Kosmochemie, Abteilung Isotopengeologie, Geowissenschaftliches Zentrum, Georg-August Universität Göttingen, Goldschmidtstraße 1, D-37077 Göttingen, Germany.
E-mail address: apack@uni-goettingen.de (A. Pack).

0016-7037/$ - see front matter © 2007 Published by Elsevier Ltd.
doi:10.1016/j.gca.2007.07.010

the chemical evolution of our part of the galaxy 4.6 Ga ago, i.e., ~8.4 Ga after the start of the cosmos (Freedman et al., 2001). Anomalous high Y/Fe-ratios in ultra metal-poor stars cannot be explained by the *r*-process only, but require an additional nucleosynthetic process that operated in the early stages of our galaxy (Burris et al., 2000). Fröhlich et al. (2006) suggested that a further process contributed to formation of some *n*-capture elements, including Y. This process, termed *vp*-process, includes antineutrino absorption in proton-rich supernova ejecta to produce a higher abundance of neutrons, which are available for producing elements with $Z > 64$, namely Sr, Y, and Zr. This process is also discussed to explain the solar system abundances of proton-rich nuclei ^{92}Mo, ^{94}Mo, ^{96}Ru, and ^{98}Ru (Dauphas et al., 2004a). According to this new model, Y formed by stellar *s*- and primordial *r*- and *vp*-processes, respectively.

In contrast to Y, 93% of solar system Ho is produced by the *r*-process with only 7% *s*-process contribution (Burris et al., 2000). A *r*-process origin of Ho is supported by the observation of Ho II absorption features in old metal-poor stars (Lawler et al., 2004) that are too old to contain *s*-process nuclides. The *vp*-process is not important for Ho.

As result of the non-cogenetic nucleosynthetic origin of Y and Ho, it is not expected that dust in the interstellar medium show a constant Y/Ho-ratio. Different condensation behavior between Y and Ho during dust condensation (e.g., Kornacki and Fegley, 1986, for condensation from a solar gas) could lead to a further separation of these elements in interstellar dust grains.

1.2. Cosmochemistry of Y and Ho

1.2.1. CI1 chondritic Y and Ho abundances

Y and Ho are both trace elements in chondrites and their components. Lodders (2003) reported concentrations of Y and Ho of 1.53 ± 0.24 and 0.0562 ± 0.0024 μg/g, respectively, for the CI1 meteorites ($Y/Ho = 27.2 \pm 4.4$, 2σ). Palme and Jones (2004) suggested in their compilation of CI1-chondrite analyses mean concentrations of 1.56 ± 0.09 μg/g Y and 0.0567 ± 0.024 μg/g Ho ($Y/Ho = 27.5 \pm 5.6$, 2σ). Concentrations of Y and Ho in the CI1-meteorites are suggested to be representative for the composition of the bulk inner solar system condensable material (Palme and Jones, 2004).

1.2.2. Fractional condensation

In terms of high-temperature cosmochemistry, Y and Ho are not regarded as twin elements (see Section 1.3.1). They were suggested to fractionate during high-temperature condensation (Boynton, 1975; Kornacki and Fegley, 1986). Boynton (1975) classified Y as a super-refractory element with a condensation temperature that is ~30 K higher than that of Ho. The very first, so-called ultrarefractory condensates (Boynton and Frazier, 1980) are hence expected to be enriched in Y relative to Ho. Condensates that form in a nebular reservoir from which the ultrarefractory component has been removed have a complementary REE pattern and should be enriched in Ho relative to Y (CAIs with Group-II REE patterns, Davis and Grossman, 1979). The difference in volatility of Y and Ho is of the same order of magnitude as the difference in the volatilities of heavy REEs that are more refractory than light REEs. Volatility controlled heavy to light REE fractionation is well established by both condensation calculations and observation of early solar system condensates (Boynton, 1975; Boynton and Frazier, 1980; Kornacki and Fegley, 1986; Boynton, 1989; Lodders, 2003).

If Y and Ho fractionate during condensation, these elements, as the REEs, can give information about fractional condensation processes during formation of the solar system's first solids at temperatures exceeding those at which REEs condense. Identification of Y/Ho-fractionation requires knowledge of the solar system Y/Ho-ratio.

1.3. Geochemistry of Y and Ho

1.3.1. The concept of geochemical twins

The elements Y and Ho are so-called geochemical twins. Y and Ho occur exclusively as trivalent cations in rocks and silicate melts and have very similar ionic radii of 1.019 (Y^{3+}) and 1.015 Å (Ho^{3+}), respectively (hexahedral coordination, Shannon, 1976). Due to their identical charge and similar ionic radius, no large fractionation among twin elements is expected during high-temperature magmatic and metamorphic processes (Goldschmidt et al., 1925; Blundy and Wood, 2003).

The coupling of Y and Ho (termed CHARAC-behavior; CHArge- and RAdius-Controlled) is observed in MORB and OIB samples that show wide variations in Y- and Ho-concentrations, but were analyzed having an average $Y/Ho = 28$ (Jochum et al., 1986a) and, more recently, to $Y/Ho = 26.4$ (Dulski, 2001). Komatiites and peridotite xenoliths have an average Y/Ho-ratio of 26 (Jochum et al., 1989). These values are within analytical error of the Y/Ho-ratio of 27 given for the CI1-meteorites (Lodders, 2003; Palme and Jones, 2004) and indicate that major planetary differentiation processes (core separation, crust formation) did not lead to large fractionation between Y and Ho.

1.3.2. High-temperature geochemistry of Y and Ho

Using available Y and Ho concentration data of international igneous rock standards, Bau (1996) defined an Y/Ho CHARAC-range of ~24–36. Non-CHARAC behavior of Y and Ho, however, is observed in some highly evolved magmas (e.g., granites, rhyolites, and pegmatites). Bau (1996) suggested that non-CHARAC behavior of Y/Ho and Zr/Hf in evolved magmas is due to complexing of these high field strength elements in the volatile-rich melts that were suggested to behave similar to aqueous solutions. In contrast, Linnen and Keppler (2002) suggested that mineral/melt Zr/Hf-fractionation is controlled by the degree of melt polymerization. Melts with high degree of polymerization (e.g., granites) show large differences in zircon and hafnon ($HfSiO_4$) activity coefficients. A similar concept may apply to the pair Y and Ho that seemingly fractionates in highly polymerized, silica-rich melts (Bau, 1996).

1.3.3. Y and Ho in aqueous systems

In contrast to most igneous rocks, large non-CHARAC Y/Ho-fractionation is observed in aqueous systems (Bau and Dulski, 1995; Bau, 1996). Strong deviation from CHARAC-controlled behavior of Y and Ho in aqueous systems is due to specific chemical complexation processes in the aqueous medium and/or adsorption on mineral surfaces (e.g., Bau, 1999). Examples of natural materials with large, non-chondritic Y/Ho-ratios are seawater (Y/Ho = 40–70, Byrne and Lee, 1993; Zhang et al., 1994; Nozaki et al., 1997), marine chemical sediments like dolomite (Y/Ho = 62.3; JDO-1 geostandard), banded iron formations (BIF; Y/Ho = 44.8; IF-G geostandard) or deep-sea ferromanganese nodules (Y/Ho ≈ 17.5; GSPN-2, GSPN-3, and NOD-P-1 geostandards, Dulski, 2001).

2. SAMPLING

2.1. Bulk meteorite samples

Meteorite material was provided from the collections at the Australian National University (ANU), the Muséum National d'Histoire Naturelle in Paris and the Senckenbergmuseum in Frankfurt (Table 1). Sample material was provided in form of a number of small fragments or a single piece.

2.2. Polished sections for spot analyses

Sampling locations were identified on previously prepared back-scattered electron maps of entire polished sections of five different unequilibrated chondrites. We report 75 LA-ICPMS analyses of Y and Ho from 36 different chondrules from unequilibrated ordinary (Chainpur, LL3.4; Dar al Gani 369, H/L3; Dar al Gani 378, H/L3) and carbonaceous (Allende, Vigarano, CV3) chondrites, respectivey. Sixteen analyses of REEs and Y are reported from 7 different CAIs and CAI-fragments. Brief sample descriptions along with Y and Ho concentration data are listed in Table 3. A part of the objects were subject of previous studies (Pack et al., 2004a,b, 2005). Therefore, we use the same nomenclature for objects and analysis number as in the previous publications.

Table 1
List of bulk meteorite samples

Meteorite	Type	Mass [g]	Source
Orgueil[a]	CI1	0.432	MHN
Murchison[a]	CM2	0.135	ANU,H
Allende[a] (A)	CV3	0.247	ANU
Allende[a] (B)	CV3	0.225	ANU
Mokoia[a]	CV3	0.140	ANU
Karoonda[a]	CK4	0.189	ANU
Chainpur[a]	LL3.4	0.309	ANU
Lake Labyrinth	LL6	1.493	ANU
St. Michel[a]	L6	0.329	ANU
Zavid[a]	L6	0.171	ANU
Hammond Downs	H4	0.248	ANU
Adrian	H4	0.612	ANU
Pultusk[a]	H5	0.090	ANU
Jilin[a]	H5	0.464	SB
Richardton[a]	H5	0.701	ANU
Forest City[a]	H5	0.750	ANU
Ijopega[a]	H6	0.383	ANU
Pillistfer[a]	EL6	0.155	ANU
Hvittis[a]	EL6	0.379	ANU

Abbreviations: "ANU" The Australian National University, Canberra, Australia; "MHN" Muséum National d'Histoire Naturelle, Paris, France; "SB" Senckenbergmuseum, Frankfurt, Germany; "H" Leibniz Universität Hannover, Germany.

[a] Observed fall.

2.3. Terrestrial lherzolite

Terrestrial spinel lherzolite GZG-1275/1 was probed as sample of the Earth mantle. Chemical and Fe-isotope data are published in Schoenberg and von Blanckenburg (2006). Using lherzolite GZG1275/1, we have prepared a chondrite analog by mixing the lherzolite powder with Fe-, Co- and Ni-powder prepared from a mixture of analytical grades metals, which contains 88.6 ± 0.7 wt% Fe, 0.35 ± 0.02 wt% Co, and 10.1 ± 0.4 wt% Ni. This mixture was used to study the influence of Ni-rich iron metal on the measurement of the Y/Ho-ratio.

Terrestrial Columbia River basalt standard USGS BCR-2G was analyzed along with meteoritical and terrestrial samples.

3. ANALYTICAL PROCEDURE

3.1. Bulk rock sample preparation

Depending on the amount of sample material available 0.15–1.5 g of bulk meteorite material (Table 1) was crushed and ground to powder in an agate mortar. Crushed material of metal-rich ordinary and enstatite chondrites and the chondrite analog, respectively, was placed in alumina crucibles in a muffle furnace (24 h at 900 °C) in order to oxidize the entire metal. At 900 °C no partial melting of meteorite material occurs, so that samples could be easily removed from the alumina crucibles without Al contamination. Oxidized material was ground to powder in an agate mortar. About 10 mg aliquots were loaded into a crucible (~4 mm inner diameter, ~4 mm deep) that was prepared from graphite rods used for spectroscopy. The powder in the crucible was gently heated and melted to a ~2 mm sphere by means of a SYNRAD 50 W CO_2 laser ($\lambda = 10.6$ μm). Samples where then placed on top of a gas stream of an aerodynamic levitation device (Nordine and Atkins, 1982) and melted without using a crucible to above liquidus (details of the technique with applications will be published elsewhere). Switching off the laser along with cooling through the gas stream ensured rapid quenching. Only the mantle lherzolite samples could be quenched to glass. Although cooling rates were ~520 K s^{-1} (~1600–600 °C) with not crucible walls present, crystallization during quenching of Fe- and Ni-rich samples could not be

avoided. Glowing of the spheres due to release of crystallization heat indicates that samples crystallized in ~0.7 s.

The small sample size allows total melting and chemical homogenization. Spheres were embedded into resin for EPMA and LA-ICPMS analyses, respectively.

3.2. Aerodynamic levitation and major element concentrations

Aerodynamic levitation as described by Nordine and Atkins (1982) provides an effective method for the preparation of homogenous samples from rock powders through melt homogenization. Two to four spheres were prepared of each material. The concentration of Ca as determined by EPMA agrees within ±5% between the individual spheres. No elemental zoning was observed within an individual sphere. Variations in Ca concentrations are, at least partly, related to variable loss of moderately volatile elements and water from the liquids. Such variations are not expected to affect the Y/Ho-ratios.

3.3. Laser ablation inductively coupled mass spectrometry

3.3.1. Bulk rock analyses

LA-ICPMS analyses (ANU) were conducted on polished sections of the fused terrestrial and meteoric rocks. The sample material was ablated using 193 nm excimer laser (112 μm beam diameter, 10 Hz, ~3 J cm^{-2}) at a scanning speed of 0.2 mm min^{-1} for 200 s. The background was measured for ~25 s before each analysis. The ablated material was transported via a He/Ar-carrier gas stream into the torch of an Aligent 7500s quadrupole ICPMS. Intensities were normalized to the intensity of ^{43}Ca. Calcium concentrations were taken from defocused (50 μm) beam EPMA. Five to eight analyses across the spheres revealed only little variation in Ca giving a mean concentration with an error that is about ±5% relative. Intensity ratios were calibrated using NIST SRM 610 with concentration values were taken from Pearce et al. (1997, Y/Ho = 1.01).

3.3.2. Precision and accuracy of analyses

The precision for the mean Y/Ho-ratio of scanning-mode analyses on BCR-2G is ±0.3% relative (2σ, $N = 7$). For single spot analyses, we obtained a precision for the mean Y/Ho-ratio of BCR-2G of ±1.1% relative (2σ, $N = 18$). The accuracy of the analyses has been tested by comparison of our data with available literature data. Fig. 1 illustrates that our data are accurate within the error of a compilation of previous analyses (data from Jochum et al., 2005). No effect of Fe, Co, and Ni in the matrix of lherzolite GZG 1275/1 on Y/Ho is observed.

3.3.3. In situ analyses of chondrite components

Spot analyses (ANU) were conducted on polished sections with spot diameters between 32 and 56 μm. The background was measured for 40 s before ablating the material. Ablation times varied with material and thickness of the section up to 40 s. Intensities were normalized to ^{29}Si with Si concentrations from EPMA. For calibration of the element to Si ratios, NIST SRM 612 glass was used. Analyses of mixtures of minerals were normalized to 100 wt% of major and minor element oxides (SiO_2, MgO, CaO, Al_2O_3, FeO, and TiO_2) from LA-ICPMS that were analyzed along with Y and Ho. In addition to NIST SRM 612, USGS BCR-2G was used for major element calibration. Since major element determination using LA-ICPMS has an intrinsic uncertainty of ~10%, concentrations could not be determined better than ±10% in such samples. In this study, however, we focus on the Y/Ho element ratio that is not affected by this approximation.

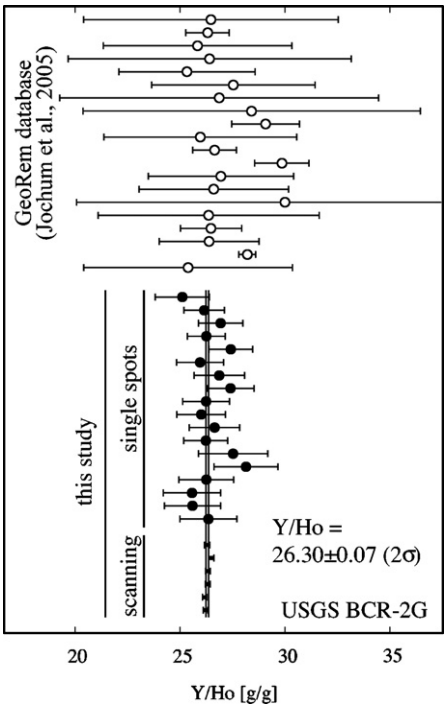

Fig. 1. Variation diagram showing the Y/Ho-ratios obtained for Columbia River basalt standard USGS BCR-2G in this study (filled symbols) in comparison with literature data (compiled by Jochum et al., 2005) on the same material.

LA-ICPMS analyses at the Natural History Museum (London) were conducted using a New Wave Research Universal Platform frequency quintupled laser ($\lambda = 213$ nm). The spot diameters were typically 70–90 μm. The background was measured for 60 s before ablation began, and ablation occurred for up to 60 s depending on the depth of the object analyzed. The ablated material was transported via a He/Ar-carrier gas to the torch of a Thermo Elemental PlasmaQuad 3 quadrupole ICPMS. Element ratios were also calibrated against NIST SRM 612 glass.

Analytical errors of individual analyses were calculated according to the procedure described by Longerich et al. (1996). Detection limits were calculated using the 3σ-criterion of the scattering of the background signal. Only 2σ errors are reported throughout the manuscript, in tables and figures. All REE-analyses are normalized using the CI1-data by Palme and Jones (2004).

4. RESULTS

4.1. Bulk meteorites

LA-ICPMS data of bulk meteorites are listed in Table 2. Super-chondritic concentrations of Y and Ho are due to loss of volatile (S, H_2O, C) and moderately volatile (K, Na) components during melting. Y and Ho are highly refractory and were not lost from the samples.

Carbonaceous chondrites (Orgueil CI1, Murchison CM2, Allende CV3, Mokoia, CV3 and Karoonda CK4) have a common Y/Ho-ratio of 25.94 ± 0.08 (2σ, $N = 15$; Fig. 2). Data of Orgueil only give Y/Ho = 25.95 ($N = 4$).

Ordinary chondrites were grouped into LL, L, and H. Two LL-chondrites (Chainpur LL3.4 and Lake Labyrinth LL6) have a slightly higher Y/Ho-ratio than carbonaceous chondrites with $Y/Ho = 26.06 \pm 0.06$ (2σ, $N = 5$; Fig. 2). L- and H-chondrites (Zavid L6, St. Michel L6, Richardton H5, Forest City H5, Jilin H5, Ijopega H6) are indistinguishable in their Y/Ho-ratio with an average value of 26.28 ± 0.05 (2σ, $N = 12$; Fig. 2), which is significantly higher than the Y/Ho-ratio of carbonaceous and LL-chondrites, respectively.

The highest Y/Ho-ratio is observed for EL6 enstatite chondrites (Pillistfer, Hvittis) with an average value of 27.25 ± 0.14 (2σ, $N = 4$, Fig. 2).

Table 2
List of fused bulk meteorite samples that were analyzed using the LA-ICPMS facility at The Australian National University (ANU, all data are normalized to Ca from EPMA)

Meteorite	Type	Analysis	Ho [μg/g] 2σ	Y [μg/g] 2σ	Y/Ho 2σ
Orgueil[a]	CI1	*a*32	0.0930 ± 0.0004	2.401 ± 0.006	25.84 ± 0.12
Orgueil[a]	CI1	*b*23	0.0859 ± 0.0003	2.247 ± 0.005	26.16 ± 0.12
Orgueil[a]	CI1	*b*24	0.0952 ± 0.0004	2.466 ± 0.007	25.91 ± 0.12
Orgueil[a]	CI1	*b*25	0.0947 ± 0.0004	2.452 ± 0.006	25.90 ± 0.12
Murchison[a]	CM2	*b16*	0.0995 ± 0.0004	2.615 ± 0.006	26.28 ± 0.11
Murchison[a]	CM2	*b17*	0.1035 ± 0.0004	2.695 ± 0.007	26.04 ± 0.12
Allende[a] (a)	CV3	*a15*	0.1009 ± 0.0003	2.600 ± 0.006	25.78 ± 0.10
Allende[a] (a)	CV3	*a16*	0.0990 ± 0.0003	2.557 ± 0.006	25.83 ± 0.11
Allende[a] (a)	CV3	*a17*	0.1018 ± 0.0004	2.615 ± 0.007	25.68 ± 0.11
Alllende[a] (b)	CV3	*b*20	0.1058 ± 0.0004	2.746 ± 0.008	25.95 ± 0.12
Alllende[a] (b)	CV3	*b*21	0.1007 ± 0.0004	2.608 ± 0.007	25.89 ± 0.11
Alllende[a] (b)[b]	CV3	*b*22	0.3262 ± 0.0008	8.524 ± 0.016	26.13 ± 0.08
Mokoia[a]	CV3	*b*8	0.0919 ± 0.0003	2.368 ± 0.006	25.77 ± 0.11
Mokoia[a]	CV3	*b*9	0.1007 ± 0.0004	2.597 ± 0.007	25.79 ± 0.12
Karoonda[a]	CK4	*b14*	0.1241 ± 0.0004	3.263 ± 0.008	26.30 ± 0.11
Karoonda[a]	CK4	*b15*	0.1265 ± 0.0004	3.278 ± 0.008	25.90 ± 0.11
Chainpur[a]	LL3.4	*b*3	0.0899 ± 0.0003	2.344 ± 0.006	26.08 ± 0.11
Chainpur[a]	LL3.4	*b*4	0.0919 ± 0.0003	2.401 ± 0.006	26.14 ± 0.11
Chainpur[a]	LL3.4	*b*5	0.0930 ± 0.0003	2.418 ± 0.007	26.01 ± 0.12
Lake Labyrinth	LL6	*b18*	0.0853 ± 0.0003	2.227 ± 0.005	26.09 ± 0.11
Lake Labyrinth	LL6	*bl9*	0.0893 ± 0.0004	2.322 ± 0.006	25.99 ± 0.12
St. Michel[a]	L6	*b12*	0.0818 ± 0.0003	2.153 ± 0.006	26.31 ± 0.12
St. Michel[a]	L6	*b13*	0.0912 ± 0.0003	2.401 ± 0.006	26.32 ± 0.12
Zavid[a]	L6	*a*30	0.0869 ± 0.0003	2.274 ± 0.005	26.17 ± 0.11
Zavid[a]	L6	*a*31	0.0874 ± 0.0003	2.313 ± 0.005	26.46 ± 0.11
Hammond Downs	H4	*a18*	0.1044 ± 0.0004	2.783 ± 0.006	26.67 ± 0.11
Hammond Downs	H4	*a19*	0.0955 ± 0.0003	2.521 ± 0.006	26.40 ± 0.11
Richardton[a]	H5	*a*20	0.0927 ± 0.0003	2.425 ± 0.006	26.16 ± 0.12
Richardton[a]	H5	*a*21	0.0890 ± 0.0003	2.340 ± 0.006	26.29 ± 0.11
Forest City[a]	H5	*a*22	0.0744 ± 0.0003	1.958 ± 0.005	26.31 ± 0.13
Forest City[a]	H5	*a*23	0.0852 ± 0.0003	2.236 ± 0.007	26.25 ± 0.12
Pultusk[a]	H5	*a*24	0.0682 ± 0.0003	1.808 ± 0.005	26.49 ± 0.13
Pultusk[a]	H5	*a*25	0.0746 ± 0.0003	1.996 ± 0.006	26.76 ± 0.13
Jilin[a]	H5	*a*26	0.0847 ± 0.0003	2.216 ± 0.006	26.17 ± 0.12
Jilin[a]	H5	*a*27	0.0813 ± 0.0003	2.136 ± 0.005	26.28 ± 0.11
Ijopega[a]	H6	*b1*	0.0776 ± 0.0003	2.043 ± 0.006	26.32 ± 0.12
Ijopega[a]	H6	*b*2	0.0742 ± 0.0003	1.955 ± 0.005	26.33 ± 0.12
Hvittis[a]	EL6	*a*28	0.0721 ± 0.0003	1.981 ± 0.005	27.48 ± 0.13
Hvittis[a]	EL6	*a*29	0.0684 ± 0.0002	1.858 ± 0.005	27.17 ± 0.12
Pillistfer[a]	EL6	*b10*	0.0578 ± 0.0002	1.571 ± 0.005	27.18 ± 0.14
Pillistfer[a]	EL6	*b11*	0.0619 ± 0.0002	1.681 ± 0.005	27.17 ± 0.12

[a] Observed fall.
[b] Sample heated with considerable degree of evaporation.

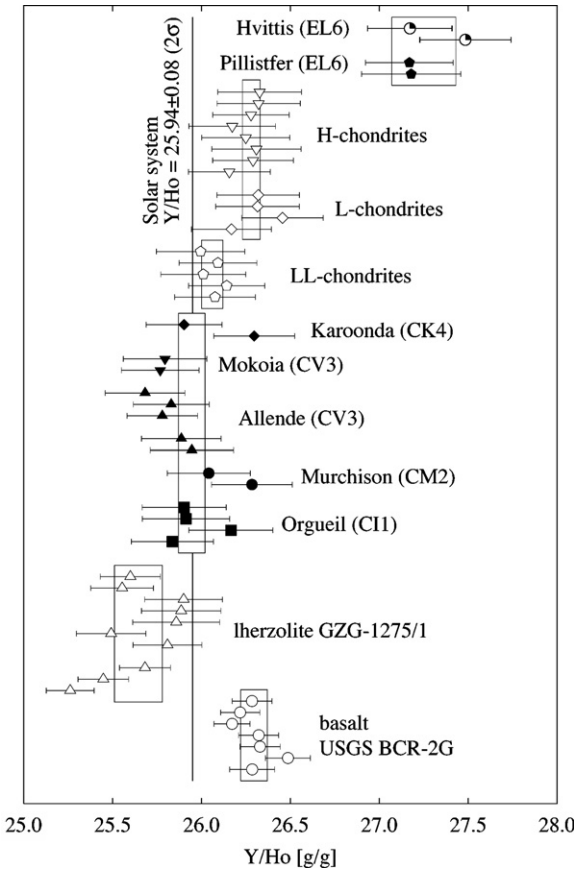

Fig. 2. Variation diagram showing Y/Ho-ratios of bulk rock samples. Displayed are data of different carbonaceous, ordinary and enstatite chondrites along with data of terrestrial lherzolite and basalt. The value for the solar system Y/Ho-ratio is indicated.

4.2. Chondritic high-temperature inclusions

4.2.1. UOC and CV3 chondrules

Concentrations of Y and Ho are highly variable in chondrules from unequilibrated ordinary and CV3 chondrites and span a range of two orders of magnitude (Table 3A, Fig. 3). No chondrule shows significant deviation from the trend in the Ho vs. Y diagram. The weighted mean Y/Ho-ratio is calculated from chondrule analyses to $Y/Ho = 26.22 \pm 0.40$ (2σ). Within error, this value overlaps with data for bulk carbonaceous and ordinary chondrites, but is significantly lower than the Y/Ho-ratio of EL6 chondrites.

Due to the larger analytical uncertainty, the difference of Y/Ho between CV3 and ordinary chondrites is not resolved in our chondrule data. Neither exists a resolvable difference of the Y/Ho-ratio between analyses from the two laboratories. Analyses obtained at ANU give a mean $Y/Ho = 25.71 \pm 0.81$ (2σ, $N = 17$) for UOC and 26.7 ± 2.6 (2σ, $N = 6$) for Allende and Vigarano chondrules, respectively. In London, we have obtained mean Y/Ho-ratios of 25.96 ± 0.56 (2σ, $N = 38$) for Allende and 27.1 ± 1.1 (2σ, $N = 11$) for Vigarano chondrules.

4.2.2. CAIs

CAI-analyses from Allende and Vigarano (CV3) span a wide range in Y and Ho and show variability in Y/Ho from 3.3 up to the carbonaceous chondrite Y/Ho-ratio of 25.94 (Table 3B, Fig. 4).

CAI-01 and CAI-fragment UFO from Vigarano both plot on the bulk carbonaceous chondrite-defined Y/Ho-ratio. CAIs CAI-01 and CAI-03 from Allende also have an Y/Ho-ratio close to 26. Two analyses from Allende CAI-02 fall on a line that defines a Y/Ho-ratio of 20.9. Two analyses of Allende CAI AC3 fall on line with a Y/Ho-ratio of only 11.1. Allende CAI AS4 shows the lowest Y/Ho-ratio of 3.3. The outer parts of that CAI have higher Y/Ho-ratios. None of the analyzed CAIs shows $Y/Ho > 26$ (Fig. 4).

In order to identify volatility-controlled refractory lithophile element fractionation, we show REE-patterns of all analyzed CAIs (Fig. 5a–f).

Allende CAI-01 shows REE abundances resembling a Group-III pattern with negative Yb-anomaly, but variable Eu (Fig. 5a). The distribution of Eu is mineralogy-controlled with Eu being enriched in melilite ($Åk_{12}$), but depleted in the coexisting perovskite- and spinel-rich region. Yb is similarly depleted in both phases, which shows that this anomaly is not controlled by the mineralogy, but volatility. Although REEs indicate volatility-controlled refractory element distribution, CAI-01 does not show significant deviation from the carbonaceous chondrite defined Y/Ho-value (Fig. 4). The REE pattern of Allende CAI-02 (Fig. 5b) is characterized by a negative Eu-anomaly and by indication of a depletion in REEs heavier than Dy. Ce shows a small positive anomaly in both analyses. This CAI shows a small negative deviation from chondritic Y/Ho with a ratio of 20.9 (Fig. 4). Unfractionated REEs are observed in Allende CAI-03 (Group-V REE pattern, Fig. 5c) and shows chondritic Y/Ho (Fig. 4). Allende AS4 is a CAI that is characterized by a distinct Group-II REE pattern and is depleted in the heavy REEs (>Eu, Fig. 5d). This CAI shows a strong Y/Ho-fractionation with a ratio of 3.3 in the core region (Fig. 4). Allende CAI AC3 from shows a REE-pattern resembling that of CAI AS4, only with a lower total REE abundance (Fig. 5e). As for AS4, it is depleted in the heavy REEs and depleted in Y relative to Ho (Fig. 4).

The melilite ($Åk_{\sim 38}$) CAI fragment UFO from Vigarano shows a continuous decrease in REE-concentrations from La to Lu, possibly with small positive Tm- and Yb-anomalies (Fig. 5f). CAI-01 from Vigarano shows a strong positive Eu-anomaly with largely unfractionated REEs (Fig. 5f). The apparent negative Lu-anomaly has not been observed in any other CAI or chondrule. An explanation cannot be given here. Both objects (UFO, CAI-01) do not show fractionated Y/Ho (Fig. 4).

4.3. Y/Ho in terrestrial materials

4.3.1. Terrestrial lherzolite GZG 1275/1 and Columbia River basalt (USGS BCR-2G)

The mean Y/Ho-ratio of spinel lherzolite sample GZG 1275/1 gives a Y/Ho-ratio of 25.65 ± 0.14 (2σ, $N = 10$). This value is by −1.1% lower than the carbonaceous chondrite Y/Ho-ratio. Seven scanning-mode analyses for USGS

Table 3A
List of samples that were analyzed using the LA-ICPMS facility at The Australian National University (ANU)

Meteorite	Type	Object	Analysis	Description	Ho [μg/g] 2σ	Y [μg/g] 2σ	Y/Ho 2σ
Chondrules							
Chainpur	LL3.4	Chal-GC	a	C	0.11 ± 0.01	3.0 ± 0.1	27 ± 3
Chainpur	LL3.4	Chal-GC	b	C	0.12 ± 0.01	3.0 ± 0.1	25 ± 3
Chainpur	LL3.4	Chal-GC	c	C	0.11 ± 0.01	3.0 ± 0.1	26 ± 3
Chainpur	LL3.4	Chal-GC	d	C	0.11 ± 0.01	2.9 ± 0.1	28 ± 3
Chainpur	LL3.4	Chal-COl	c	PO	0.88 ± 0.08	22 ± 1	25 ± 3
Chainpur	LL3.4	Chal-A	b	PO	0.38 ± 0.04	9.1 ± 0.3	24 ± 3
Chainpur	LL3.4	Chal-B	d	PO	0.26 ± 0.02	6.8 ± 0.2	26 ± 3
Dar al Gani 369	L/H3	D369-A	a	C	0.06 ± 0.01	1.6 ± 0.1	27 ± 5
Dar al Gani 369	L/H3	D369-B	a	C	0.09 ± 0.01	2.2 ± 0.1	24 ± 4
Dar al Gani 378	H/L3	D378-RF05	a	PO	0.33 ± 0.04	8.8 ± 0.6	26 ± 4
Dar al Gani 378	H/L3	D378-RF10	a	BO	0.28 ± 0.02	7.0 ± 0.2	25 ± 2
Dar al Gani 378	H/L3	D378-RF10	b	BO	0.28 ± 0.03	7.7 ± 0.2	27 ± 3
Dar al Gani 378	H/L3	D378-RF01	b	PO	0.52 ± 0.08	13.3 ± 2.0	25 ± 6
Dar al Gani 369	L/H3	D369-RF02	b	PO	0.45 ± 0.06	12.8 ± 0.6	29 ± 4
Dar al Gani 369	L/H3	D369-RF02	c	PO	0.93 ± 0.07	22.7 ± 0.5	24 ± 2
Dar al Gani 369	L/H3	D369-RF02	d	PO	0.78 ± 0.16	22.2 ± 1.2	28 ± 6
Dar al Gani 378	H/L3	D378-RF03	a	PO	0.34 ± 0.05	10.1 ± 0.6	30 ± 5
Allende	CV3	A11K1-CH01	b	PO	0.48 ± 0.03	13.5 ± 0.7	28 ± 2
Vigarano	CV3	Vigl-RFIO	b	MPO	0.77 ± 0.07	22.3 ± 0.6	29 ± 3
Vigarano	CV3	Vigl-RF17	b	PO	0.20 ± 0.02	5.7 ± 0.1	28 ± 3
Vigarano	CV3	Vigl-RF14	c	BO	0.23 ± 0.03	5.8 ± 0.5	25 ± 4
Vigarano	CV3	Vigl-RF14	d	BO	0.12 ± 0.02	2.7 ± 0.1	23 ± 3
Vigarano	CV3	Vigl-RF14	e	BO	0.17 ± 0.02	4.4 ± 0.2	25 ± 3
Ca- andAl-rich inclusions							
Allende	CV3	A11K1-CAI01	a	CAI, mel+spl	5.6 ± 0.8	131 ± 16	23 ± 4
Allende	CV3	A11K1-CAI01	b	CAI, mel+spl	0.24 ± 0.04	6.9 ± 0.3	29 ± 5
Allende	CV3	A11K1-CAI03	a	CAI,–	0.12 ± 0.01	3.2 ± 0.2	27 ± 4
Allende	CV3	A11K1-CAI03	b	CAI,–	0.14 ± 0.02	3.4 ± 0.5	23 ± 5
Allende	CV3	A11K1-CAI03	c	CAI,–	0.09 ± 0.01	2.2 ± 0.2	25 ± 5
Allende	CV3	A11K1-CAI02	a	CAI, mel+spl	10.0 ± 0.8	200 ± 9	20 ± 2
Allende	CV3	A11K1-CAI02	b	CAI, mel+spl	0.95 ± 0.08	20.7 ± 0.7	22 ± 2
Vigarano	CV3	Vig1-CAIOl	—	CAI, mel+spl+high-Ca px	0.29 ± 0.03	7.2 ± 0.2	25 ± 3
Vigarano	CV3	Vig1-UFOl	—	CAI- fragment, high-Ca px	0.80 ± 0.05	20.6 ± 0.6	26 ± 2

Abbreviations: C, cryptocrystalline chondrule; MPO, macroporphyritic chondrule; PO, porphyritic olivine chondrule; BO, barred olivine chondrule.

BCR-2G basalt give a mean Y/Ho = 26.30 ± 0.08 (2σ). Eighteen spot analyses on BCR-2G give a weighted mean Y/Ho-ratio of 26.44 ± 0.28 (2σ), which is within error identical to the scanning-mode analyses. Combining scanning-mode and spot analyses gives Y/Ho = 26.30 ± 0.07 (2σ) for BCR-2G, which is +1.9% higher than the carbonaceous chondrite defined Y/Ho-ratio.

5. DISCUSSION

5.1. Bulk rock sample preparation technique

Fusion of <20 mg of bulk rock powders by means of laser assisted heating and aerodynamic levitation in combination with LA-ICPMS is shown to be a rapid technique that allows high-precision analyses of refractory elements and their ratios in geological and meteoritical samples. Using this technique, we report data of the Y/Ho-ratio of unprecedented precision with relative uncertainties <1%. The disadvantage of the technique is the loss of moderately volatile (e.g., Na, K) and volatile (e.g., H_2O, S) elements from the samples.

5.2. Cosmochemistry of Y and Ho

5.2.1. Solar system Y/Ho-ratio

Our chondrite data show that there is not a single chondritic Y/Ho-ratio. Y/Ho-fractionation obviously occurred on a large scale in the solar nebula on the scale of reservoirs from which the different chondrites source.

Carbonaceous chondrites (CI1, CM2, CV3, and CK4) have a common Y/Ho-ratio of 25.94 ± 0.08 (2σ). Jochum et al. (1986b) reported a Y/Ho-ratio of 28.1 ± 4 (2σ) for Orgueil.[1] The CI1 chondrite Y/Ho-ratio adopted in the compilations by Lodders (2003) and Palme and Jones (2004) is Y/Ho = 27.5 ± 5.7 (2σ). For eight carbonaceous chondrites (CI1, CM2, and CV3), Jochum et al. (1986b) gave a mean Y/Ho-ratio of 28.9 ± 4 (2σ).

[1] Jochum et al. (1986b) give a relative error of the Y and Ho concentrations of <6% relative (1σ) We have assumed an uncorrelated 2σ error of ±10% for both elements.

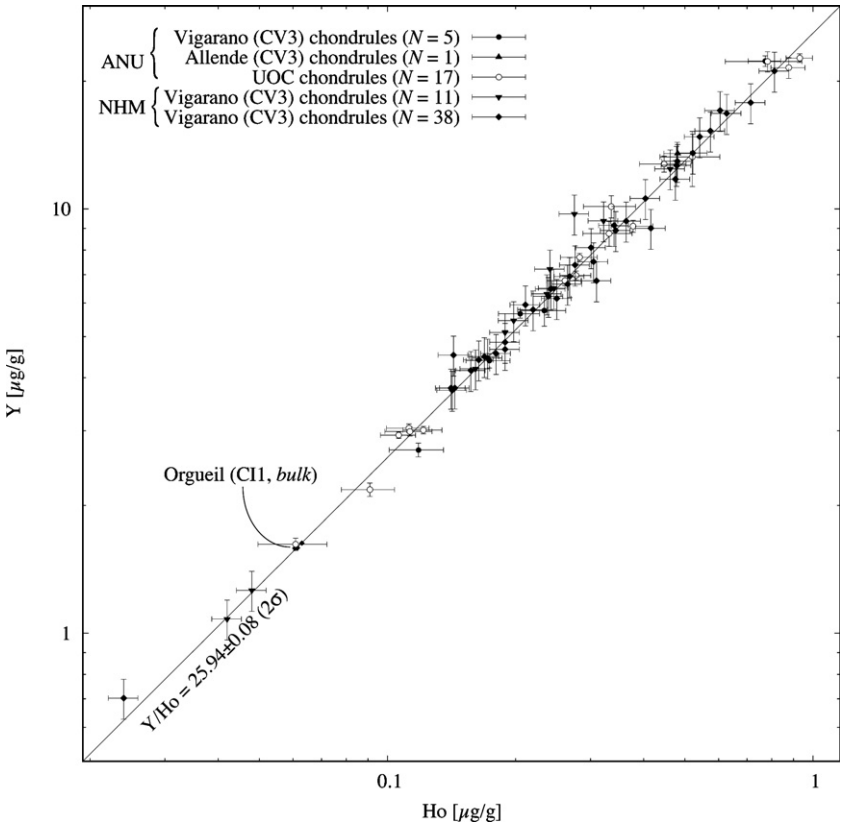

Fig. 3. Plot of Ho vs. Y of 72 LA-ICPMS analyses of chondrules from UOCs (Chainpur, LL3.4; Dar al Gani 369, L/H3; Dar al Gani 378, H/L3) and CV3 chondrites (Vigarano; Allende). The weighted mean Y/Ho is 26.22 ± 0.40 (2σ). CI1-chondrite data are from this study (Orgueil, data normalized to Ca concentration given by (Lodders, 2003)).

The CI1 carbonaceous chondrite Orgueil has a Y/Ho-ratio that is indistinguishable from the mean carbonaceous chondrite value. CI1 chondrites have, with exception of the volatile elements, a chemical composition that is similar to the composition of the Sun (Palme, 2001; Lodders, 2003; Palme and Jones, 2004). We therefore conclude that the carbonaceous chondrite Y/Ho-ratio is representative for the Y/Ho-ratio of the bulk solar system that is 25.95 ± 0.08 (2σ). The uncertainty of our new estimate is 0.3%, i.e., reduced by more than one order of magnitude compared to any previous study.

5.2.2. Origin of Y/Ho-fractionation among chondrite groups

Data for ordinary (LL, L, and H) and EL6 enstatite chondrites reveal significant deviation from the solar Y/Ho-ratio (Fig. 2). LL-chondrites have a Y/Ho-ratio that is +0.5% higher than the solar value. L- and H-chondrites have a common Y/Ho-ratio that is +1.3% higher than the solar value. The highest Y/Ho-ratio is measured in the two analyzed EL6 enstatite chondrites, for which Y/Ho deviates by +5.1% from the solar value.

The bulk major element compositions of carbonaceous, ordinary and enstatite chondrites are somewhat similar (Jarosewich, 1990). All chondrites containing significant amounts of free metal were oxidized prior to fusion. Also, addition of Fe, Ni, Co metal to lherzolite did not result in systematic change in measured Y/Ho. Therefore an analytical artifact due to different matrices is excluded.

We have demonstrated in section 1.1 that Y/Ho do have different nucleosynthetic origins and are not expected to occur in constant ratios in the material of the interstellar medium. In addition, fractional condensation of dust in stellar atmospheres could lead to further separation of Y from Ho. A higher abundance in Y relative to Ho could suggest a slightly higher *s*- and/or *vp*-process component (Y) relative to the *r*-process component (Ho) in ordinary chondrites and especially enstatite chondrites. If present, such variations should be detectable in terms of isotope heterogeneity. Remarkable isotopic homogeneity of solar system materials of different provenances (e.g., Zhu et al., 2001; Bizzarro et al., 2004), however, indicates that only a very small component (i.e., presolar grains, Nittler, 2003) was directly inherited from the ISM.

We conclude that the variability in Y/Ho was probably not inherited from the ISM, but is result of fractionation processes within the solar nebula. Calculations by Kornacki and Fegley (1986) suggest that Y/Ho-fractionation can be produced by fractional condensation in the solar nebula. Our data (Fig. 4) and data from the literature (Fig. 6b) demonstrate separation of Y from Ho in some refractory inclusions. REEs in CAIs suggest formation by fractional condensation and/or evaporation (Boynton, 1975; Boynton, 1989). The data in (Fig. 6a) demonstrate that fractionation of

Table 3B
List of samples that were analyzed using the LA-ICPMS at the Natural History Museum (NHM)

Meteorite	Type	Object	Analysis	Description	Ho [μg/g] 2σ	Y [μg/g] 2σ	Y/Ho 2σ
Chondrules							
Vigarano	CV3	C2	b	PO	0.042 ± 0.003	1.1 ± 0.1	26 ± 3
Vigarano	CV3	C3	a	PO	0.16 ± 0.01	4.2 ± 0.5	26 ± 4
Vigarano	CV3	C3	b	PO	0.25 ± 0.02	6.5 ± 0.7	26 ± 4
Vigarano	CV3	C3	c	PO	0.32 ± 0.03	9.4 ± 1.0	29 ± 4
Vigarano	CV3	C4	a	PO	0.46 ± 0.04	12.4 ± 1.3	27 ± 4
Vigarano	CV3	C4	b	PO	0.048 ± 0.004	1.3 ± 0.1	26 ± 4
Vigarano	CV3	C5	a	PO	0.19 ± 0.02	5.1 ± 0.6	27 ± 4
Vigarano	CV3	C5	b	PO	0.20 ± 0.02	5.5 ± 0.6	28 ± 4
Vigarano	CV3	C5	c	PO	0.24 ± 0.02	7.2 ± 0.8	30 ± 4
Vigarano	CV3	C6	a	PO	0.28 ± 0.02	9.7 ± 1.1	35 ± 5
Vigarano	CV3	C7	a	PO	0.24 ± 0.02	6.3 ± 0.7	27 ± 4
Allende	CV3	em3	a	PO	0.21 ± 0.02	5.9 ± 0.6	28 ± 4
Allende	CV3	em3	b	PO	0.19 ± 0.02	4.8 ± 0.5	26 ± 3
Allende	CV3	em3	c	PO	0.17 ± 0.01	4.5 ± 0.5	27 ± 4
Allende	CV3	em3	d	PO	0.34 ± 0.03	9.1 ± 1.0	27 ± 4
Allende	CV3	eml	a	BO	0.42 ± 0.03	9.0 ± 1.0	22 ± 3
Allende	CV3	eml	b	BO	0.31 ± 0.02	6.8 ± 0.7	22 ± 3
Allende	CV3	eml	c	BO	0.25 ± 0.02	6.2 ± 0.7	25 ± 3
Allende	CV3	em2	a	RP	0.34 ± 0.03	8.9 ± 1.0	26 ± 3
Allende	CV3	em2	b	RP	0.27 ± 0.02	6.6 ± 0.7	25 ± 3
Allende	CV3	em4	a	PO	0.81 ± 0.07	21 ± 2	26 ± 3
Allende	CV3	em4	b	PO	0.024 ± 0.002	0.7 ± 0.1	29 ± 4
Allende	CV3	AS3	a	CC	0.22 ± 0.02	5.8 ± 0.6	26 ± 4
Allende	CV3	AS3	b	CC	0.16 ± 0.01	4.2 ± 0.4	27 ± 4
Allende	CV3	AS3	c	CC	0.16 ± 0.01	4.4 ± 0.5	27 ± 4
Allende	CV3	AS3	d	C	0.14 ± 0.01	3.8 ± 0.4	27 ± 4
Allende	CV3	AX13	a	Po	0.14 ± 0.01	4.5 ± 0.5	32 ± 4
Allende	CV3	AX13	b	PO	0.18 ± 0.01	4.6 ± 0.5	25 ± 3
Allende	CV3	AX13	c	PO	0.52 ± 0.04	14 ± 1	26 ± 3
Allende	CV3	AX13	d	PO	0.14 ± 0.01	3.8 ± 0.4	26 ± 4
Allende	CV3	AX14	a	POP	0.19 ± 0.02	4.7 ± 0.5	25 ± 3
Allende	CV3	AX14	b	POP	0.31 ± 0.02	7.5 ± 0.8	25 ± 3
Allende	CV3	AX14	c	POP	0.40 ± 0.03	10.6 ± 1.1	26 ± 4
Allende	CV3	AX14	d	POP	0.14 ± 0.01	3.7 ± 0.4	26 ± 4
Allende	CV3	AX12	a	BO	0.28 ± 0.02	7.4 ± 0.8	27 ± 4
Allende	CV3	AX12	b	BO	0.63 ± 0.05	16.8 ± 1.8	27 ± 4
Allende	CV3	AC1	a	PO	0.17 ± 0.01	4.5 ± 0.5	26 ± 3
Allende	CV3	AC1	b	PO	0.36 ± 0.03	9.4 ± 1.0	26 ± 3
Allende	CV3	AC1	c	PO	0.24 ± 0.02	6.5 ± 0.7	27 ± 4
Allende	CV3	AC1	d	PO	0.27 ± 0.02	6.9 ± 0.7	26 ± 3
Allende	CV3	AC2	a	PO	0.48 ± 0.04	11.8 ± 1.3	25 ± 3
Allende	CV3	AC2	b	PO	0.54 ± 0.04	15 ± 2	27 ± 4
Allende	CV3	AC2	c	PO	0.48 ± 0.04	13.0 ± 1.4	27 ± 4
Allende	CV3	AC4	a	BO	0.30 ± 0.02	8.1 ± 0.9	27 ± 4
Allende	CV3	AC5	a	PO	0.24 ± 0.02	6.2 ± 0.7	26 ± 4
Allende	CV3	AC5	b	PO	0.57 ± 0.05	15 ± 2	27 ± 4
Allende	CV3	AC6	a	PO	0.61 ± 0.05	17 ± 2	28 ± 4
Allende	CV3	AC6	b	PO	0.71 ± 0.06	18 ± 2	25 ± 3
Allende	CV3	AC6	c	PO	0.48 ± 0.04	13 ± 1	27 ± 4
Ca- andAl-rich inclusions							
Allende	CV3	AC3	a	CAI- fine grained Type A	0.023 ± 0.002	0.23 ± 0.03	10 ± 1
Allende	CV3	AC3	b	CAI- fine grained Type A	0.026 ± 0.002	0.32 ± 0.03	12 ± 2
Allende	CV3	AC3	c	CAI- fine grained Type A	0.08 ± 0.01	1.6 ± 0.2	20 ± 3
Allende	CV3	AS4	a	CAI, core	0.06 ± 0.01	0.21 ± 0.02	3.3 ± 0.4
Allende	CV3	AS4	b	CAI, mantle	0.043 ± 0.003	0.20 ± 0.02	4.6 ± 0.6
Allende	CV3	AS4	c	CAI, core	0.09 ± 0.01	0.29 ± 0.03	3.3 ± 0.4
Allende	CV3	AS4	d	CAI, rim	0.12 ± 0.01	1.3 ± 0.1	11 ± 1

Abbreviations: CC, compound chondrule; PO, porphyritic olivine chondrule; PR, radiating pyroxene chondrule; BO, barred olivine chondrule; POP, porphyritic olivine and pyroxene chondrule.

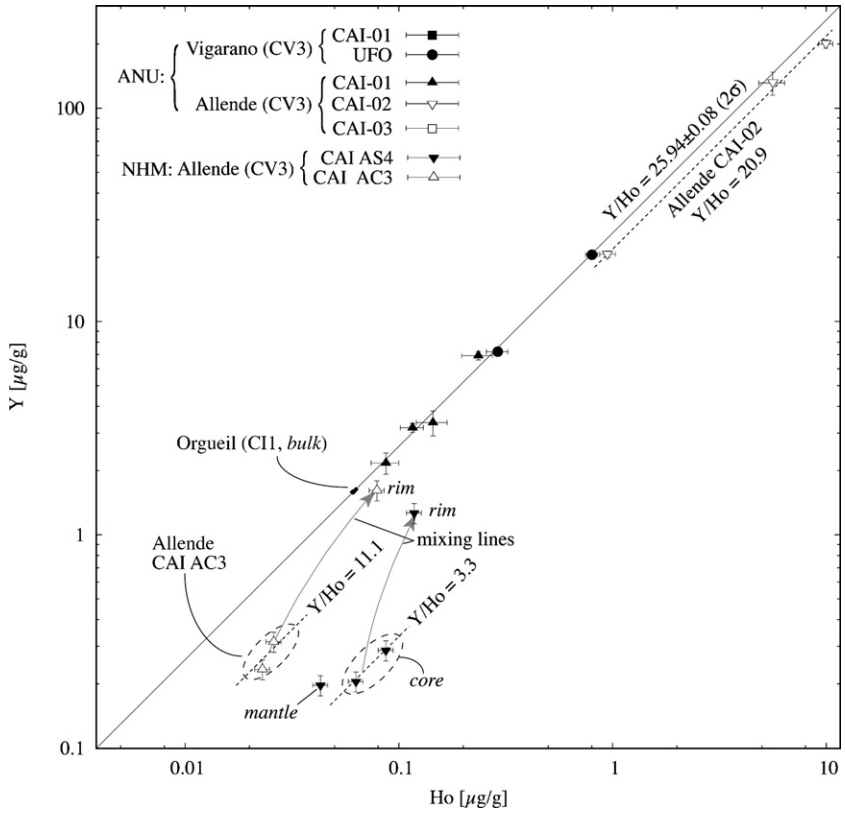

Fig. 4. Plot of Ho vs. Y of 16 LA-ICPMS analyses from CAIs from Allende and Vigarano (CV3). The CI1-chondrite values are from this study (Orgueil, data were normalized to Ca concentration given by Lodders (2003)).

Y and Ho covaries with fractionation among REEs that is believed to be understood in terms of differences in volatilities. If carbonaceous chondrites, as suggested, reflect the Y/Ho-ratio of the solar nebula, ordinary and enstatite chondrites have either accumulated a component with elevated Y/Ho or have lost a component with subsolar Y/Ho. Calculations by Kornacki and Fegley (1986) indicate that at pressures between 10^{-3} and 10^{-6} bar, Y is more refractory than Ho (gas of solar composition). The data on CAIs indicate that Y is, indeed, more refractory than Ho showing that condensation could not have occurred a pressure around 10^{-9} bar, at which Ho becomes more refractory than Y (Kornacki and Fegley, 1986). Elevated Y/Ho-ratios of chondrites can be explained by addition of super-refractory dust with super-solar Y/Ho-ratio. If this dust comprised ultrarefractory CAI-like material as shown in Fig. 6b, it would have had a Y/Ho-ratio of ~52 (2 × solar). Addition of 0.5% Y and Ho from such material would explain the Y/Ho-ratio of LL chondrites. L and H chondrites would require that 1.3% of their Y and Ho sources from ultrarefractory dust. Addition of a fraction of 5% is required to explain the elevated Y/Ho in EL6 chondrites.

The data from CAIs show that the deviation towards lower Y/Ho-ratios is much larger in CAIs with Group-II REE pattern. We report a CAI with Y/Ho = 3.3. Removal of such a component from the reservoir where the ordinary and enstatite chondrites formed would lead to a bulk composition with super-solar Y/Ho. Subtraction of 0.5, 1.5, and 5.8% Y and Ho of CAI dust (Group-II REE pattern, Y/Ho = 3.3), respectively, would explain the observed variations in bulk Y/Ho of carbonaceous, ordinary and EL6 chondrites.

We take the subsolar ratios of refractory lithophile elements Al, Ca or Ti to Si of enstatite chondrites relative to carbonaceous chondrites (Jarosewich, 1990; Palme and Jones, 2004) as argument to conclude that a refractory component was lost rather than a super-refractory component was added to the reservoir in which ordinary and enstatite chondrites formed. This component was material that presumably resembled CAIs with Group-II REE patterns. Variations among other refractory elements in bulk chondrites should mirror the loss of a refractory component.

This conclusion is supported by distinct differences in the ratios of highly refractory siderophile elements like Re and Os between chondrite groups. Walker et al. (2002) showed that bulk ordinary and enstatite chondrites have 5–7% higher Re/Os than carbonaceous chondrites. Model condensation calculations indicate that Re and Os condense among the first elements from a gas of solar composition (Palme and Wlotzka, 1976). Fegley and Palme (1985) showed that Re may be slightly more refractory than Os in a gas of solar composition and pressures between 10^{-3} and 10^{-9} bar. They treated the condensate as ideal refractory alloy, which is a major uncertainty in the calculations (Palme, 2007, pers. comm.). If fractionation of Re and Os

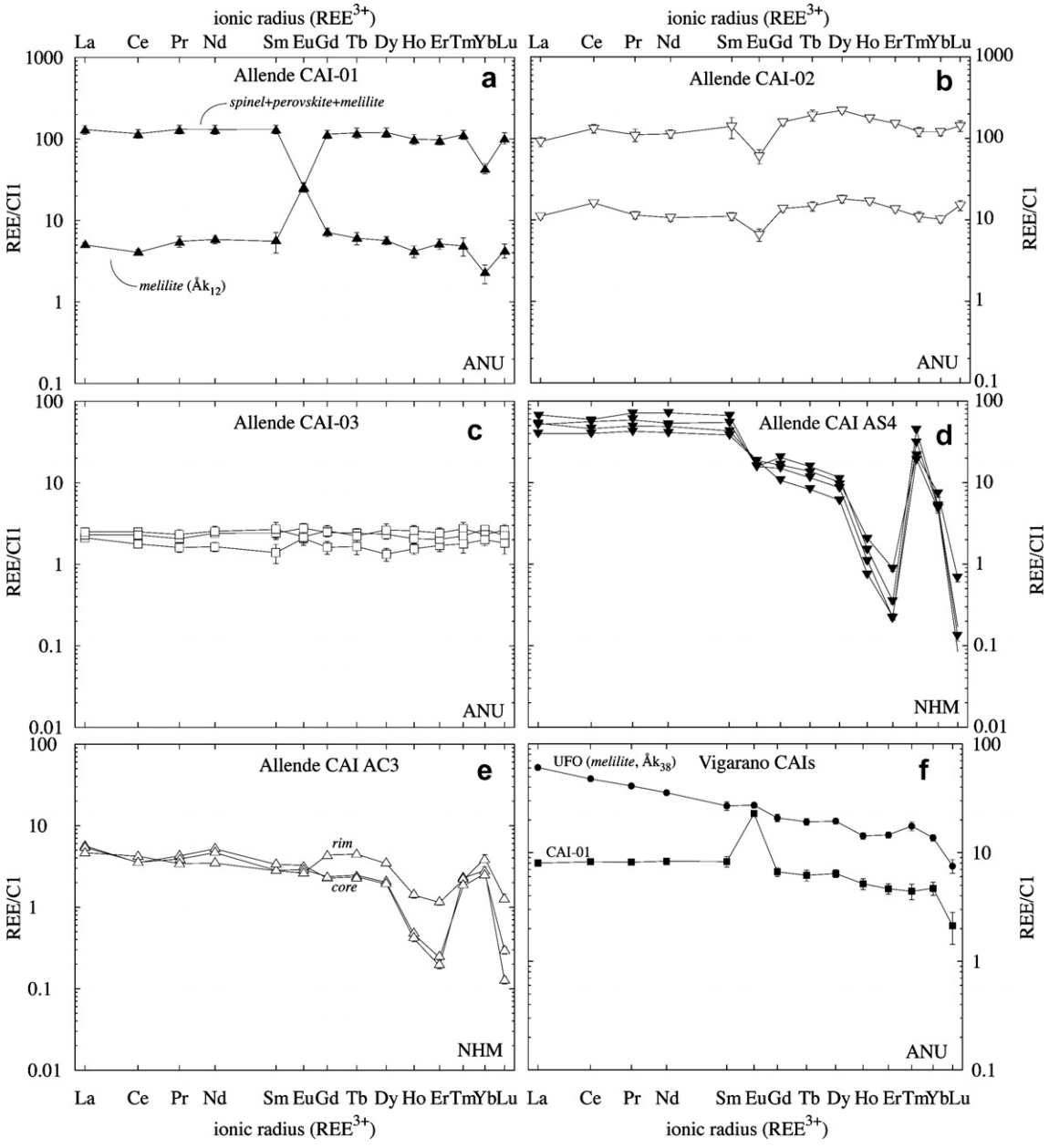

Fig. 5. (a–f) CI1 chondrite normalized REE patterns of CAIs from CV3 chondrites Allende and Vigarano.

occurred by removal of dust that was also responsible for the fractionation of Y and Ho in the residual reservoir, it seems reasonable to follow that Re is, indeed, more refractory than Os.

We conclude that the variation in refractory elements between different chondrites was established during the high-temperature stage of the early solar nebula and operated on scales of the size of the reservoirs from which the different types of chondrites formed. Fractional condensation and isolation of condensates did not only lead to fractionation among non-refractory elements (Palme, 2001), but also affected the ratios among the ultra and highly refractory elements Y and Ho, respectively.

5.2.3. Chondrules

Chondrules from two major types of the primitive meteorites (UOCs, CV3) have a common Y/Ho-ratio of 26.22 ± 0.40 (2σ, Fig. 3). This value is in good agreement to the Y/Ho-ratio of ~25 obtained by Alexander (1994) from chondrule mesostases from unequilibrated ordinary chondrites and overlaps with our solar ratio of 25.94. The limited accuracy and precision of the LA-ICPMS spot analyses does not allow identification of the small difference between the chondrite groups that has been revealed on bulk samples (see Section 4.3). No chondrule showed significant deviation from the mean Y/Ho. The Y/Ho-ratio is not a function of the amount of these elements present in chondrule phases.

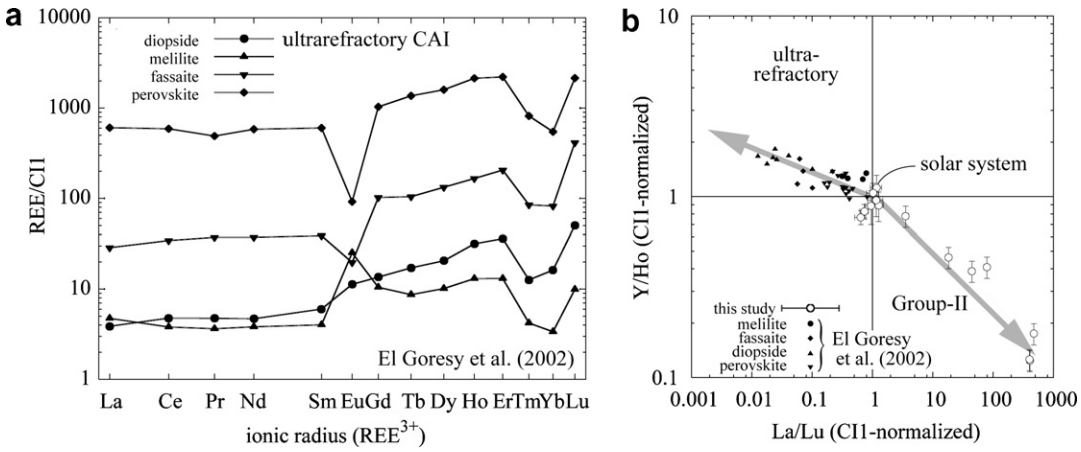

Fig. 6. (a) Mean REE-abundances in phases from an ultrarefractory CAI. Data are from a CAI from CV3-chondrite Efremovka (El Goresy et al., 2002) and were made available in tabulated form by A. El Goresy. (b) Plot of chondrite-normalized Y/Ho vs. La/Lu of CAIs from Allende and Vigarano (this study) and of phases from an ultrarefractory CAI from (El Goresy et al., 2002).

We have shown in Section 1.1 that the material from which the solar system formed was probably highly heterogeneous with respect to Y/Ho. We have concluded in the previous section that this heterogeneity is not inherited in bulk chondrites. On a percent-level scale, this heterogeneity is also not reflected in chondrule Y/Ho-ratios, although chondrules sampled 10^{-26}–10^{-20} of the mass of a whole asteroid ($m_{\text{chondrule}} \approx 1$ mg; $m_{\text{Ceres}} = 8.7 \times 10^{26}$ mg, Hilton, 1999). Individual chondrules from ordinary and carbonaceous chondrites are distinct with respect to their oxygen isotope composition (Clayton, 2004). This heterogeneity suggests that they sampled different portions of the solar nebula. Since no Y/Ho heterogeneity is observed between UOC and CC in chondrules, large-scaled homogenization on the percent-level scale pre-dates chondrule formation. This interpretation is supported by the lack of iron isotope anomalies in chondrules (Zhu et al., 2001). If chondrules formed by melting of primordial, large-scale homogeneous ISM dust, chondrules would have sampled a representative number of grains resulting in a constant Y/Ho-ratio. If heterogeneous chondrule precursors were spherical with a mean diameter of 1 μm, a spherical chondrule with a diameter of 300 μm would have sampled 2.7×10^7 dust grains. Any grain-to-grain heterogeneity would have been obliterated through the large number of grains sampled. Relict grains in chondrules were taken as evidence for recycling of chondrule material (Jones and Danielson, 1997). Chondrule recycling is a process that eventually leads to complete homogenization of the Y/Ho-ratio.

No correlation between the concentrations of Y and Ho and the Y/Ho-ratio is observed. Within error, those chondrules with the highest Y and Ho concentrations do not deviate from the solar Y/Ho-ratio. This suggests that chondrules either sampled refractory material with unfractionated Y/Ho-ratio or that contribution of CAI-like material with large Y/Ho-fractionation was limited. Mixing of CAI like material with a composition similar to the most fractionated Allende CAI AS4 (analysis #a, Table 3, Y/Ho = 3.3) with dust with CI1 chondritic Y and Ho abundances would require $\geqslant$20% CAI material to account for a Y/Ho-ratio of $\leqslant$20. Due to the limitations in accuracy and precision of single spot analyses, identification of smaller amounts of CAI material with fractionated Y/Ho is not permitted.

5.2.4. Solar nebular Y/Ho-fractionation in CAIs

Data from CAIs show that these components do not share a common value for Y/Ho (Fig. 4). Three out of seven different CAIs and CAI-fragments show significant deviation towards lower values than the solar Y/Ho-ratio, with Y/Ho as low as 3.3 (Fig. 4). CAIs that show heavy/light REE fractionation with depletion in heavy REEs are systematically depleted in Ho relative to Y (Figs. 4 and 5). The relation between light/heavy REE- and Y/Ho-fractionation is illustrated in Fig. 6. The light/heavy REE-fractionation is expressed in terms of CI1-normalized La/Lu.

CAIs that are depleted in the ultrarefractory component (i.e., having Group-II REE patterns) show super-chondritic La/Lu, but subsolar Y/Ho. The ultrarefractory component that is missing in CAIs with Group-II patterns is hence expected having super-solar Y/Ho. A CAI with characteristics of an ultrarefractory REE pattern (i.e., heavy > light REE fractionation) was described by El Goresy et al. (2002). Phases in this CAI (melilite, diopside, fassaite, and perovskite) all display subchondritic La/Lu and super-solar Y/Ho (Fig. 6). Fractionation of Y and Ho in the very first condensates indicates that Y is, indeed, more refractory than Ho as suggested by condensation calculations by Kornacki and Fegley (1986).

5.3. Y/Ho of the Earth and fractionation in terrestrial igneous rocks

5.3.1. Lherzolite GZG-1275/1 and Columbia River basalt BCR-2G

We have obtained a Y/Ho-ratio of 25.65 ± 0.14 for mantle lherzolite sample GZG-1275/1. This value is +1.2% lower than the solar ratio of 25.94. The REE pattern as well as the major element chemical composition indicates that the studied lherzolite experienced one or more partial

melting events. It is shown that Columbia River basalt BCR-2G has a Y/Ho-ratio of 26.30 ± 0.07 (2σ), which is 1.4% higher than the solar value. Partial melting and loss of a basaltic component with elevated Y/Ho is a feasible process that may have lowered the Y/Ho-ratio of the depleted mantle. For the bulk silicate Earth (BSE), a Y/Ho-ratio identical to that of carbonaceous chondrites (25.94 ± 0.08, 2σ) is suggested. The Y/Ho-ratio of the Earth is much lower than the Y/Ho-ratio of enstatite chondrites, which questions models describing the Earth as of having accreted from enstatite chondrites (Javoy, 1995; Herndon, 1996). Instead, our data support the view that the Earth formed from material that resembled carbonaceous chondrites (Palme and Nickel, 1985; Palme, 2001). Recent high-precision Cr isotope data by Trinquier et al. (2007), however, could support the relation between Earth and enstatite chondrites. Since the origin of the ^{54}Cr isotope anomaly is not yet well understood and since that there exists major differences between Earth and enstatite chondrites (e.g., Fe/FeO-ratio), we conclude that the Earth is rather related to carbonaceous chondrites than to enstatite chondrites.

5.3.2. Behavior of Y and Ho during igneous differentiation

Fig. 7 shows a compilation of solution ICPMS data of igneous rock standards by Dulski (2001) and Jochum et al. (2005). Since Dulski (2001) obtained all data by means of the same method (solution ICPMS) and since his Y/Ho-ratio in BCR-1 and our Y/Ho-ratio in BCR-2G do not show a resolvable difference, we regard our and his data sets as being consistent.

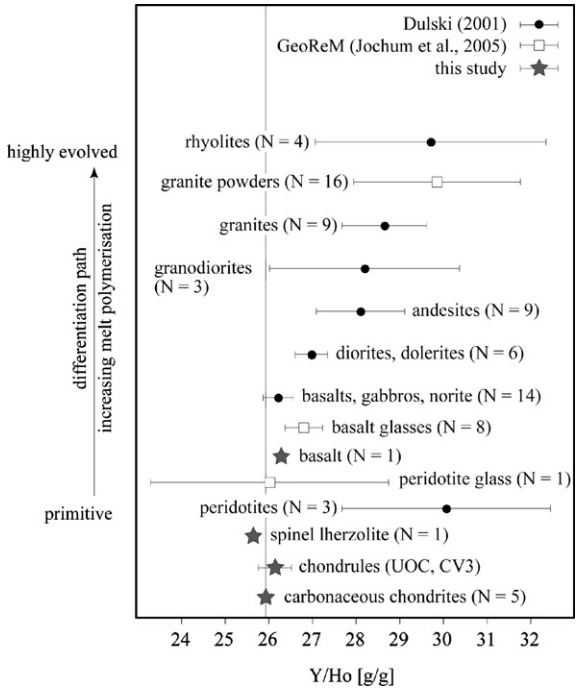

Fig. 7. Variation diagram showing the Y/Ho-ratio of different igneous rock types (data from Dulski, 2001, and from this study). Data are arranged in order of increasing degree of melt of differentiation.

The compilation Y/Ho shows a systematic increase from mafic rock over intermediate rocks to highly evolved rocks (granites and rhyolites) that have Y/Ho ≈ 28–30. On smaller scale, igneous fractionation of Y and Ho between spinel lherzolite and basalt is observed in this study. Our data along with literature data of more felsic rocks show that during partial melting, Y is less compatible than Ho and is enriched in the melt. The variability in Y/Ho shows an increase with increasing degree of evolution. Although highly evolved rocks generally have elevated Y/Ho, Bau (1996) demonstrated that granites can span a very large range from super- down to subsolar Y/Ho-ratios.

Notably, none of the igneous rock standards shows subsolar Y/Ho-ratios. Assuming a BSE with solar Y/Ho, a component with subsolar Y/Ho is missing. It was shown that deep-sea ferromanganese nodules have subsolar Y/Ho (Dulski, 2001). Such materials, however, are rare and are not regarded as the missing complementary component to the felsic rocks. Our data of lherzolite and basalt show that partial melting lowers the Y/Ho-ratio in residual rocks. We suggest that residual rocks (restites) may be the missing component that outbalances the super-solar Y/Ho-ratio of felsic igneous crustal rocks.

5.3.3. Y and Ho in the Earth crust–zircon

Zircon ($ZrSiO_4$) is a widespread accessory mineral in the majority of igneous rocks, excluding peralkaline rocks that form from melts with too high zircon solubility. Since the Y and Ho budget of igneous rocks is largely dominated by zircon crystallization, Y/Ho analyses in zircon may be a good proxy for the Y/Ho of the bulk rock. High concentrations of Y and Ho in zircons enable determination of Y/Ho with relatively low analytical error. Belousova et al. (2002) published LA-ICPMS analyses of a large set of zircons from different geological settings. Their data are displayed in Fig. 8. Although Y and Ho concentrations vary by approximately four orders of magnitude (Fig. 8a), igneous zircons show limited variability in their Y/Ho-ratio of between 23 and 34 (includes 95% of all data, Fig. 8b). The average Y/Ho-ratio in zircons is ~28, which is slightly higher than the solar Y/Ho-ratio. The elevated Y/Ho-ratio could be due to the origin of most zircons from felsic rocks that have been shown to have supersolar Y/Ho (Fig. 7). We suggest that this variability reflects the combined variability of their host rocks, as shown in Fig. 7. The solar Y/Ho-ratio is well within the variability of terrestrial zircons (Fig. 8b). The maximum of the Y/Ho-distribution of terrestrial zircons (~29) coincides with the average ratio in silica-rich igneous rocks (Fig. 7).

5.3.4. CHARAC-behavior of Y and Ho in igneous systems?

Our data, along with data compiled from Dulski (2001) demonstrate that the pair Y/Ho is, compared to other pairs like Zr/Hf and Nb/Ta, the most robust geochemical twin. Variations of Zr/Hf and Nb/Ta in terrestrial igneous rocks are higher by an order of magnitude (Münker et al., 2003) than variations of the Y/Ho-ratios in igneous rocks reported in this study.

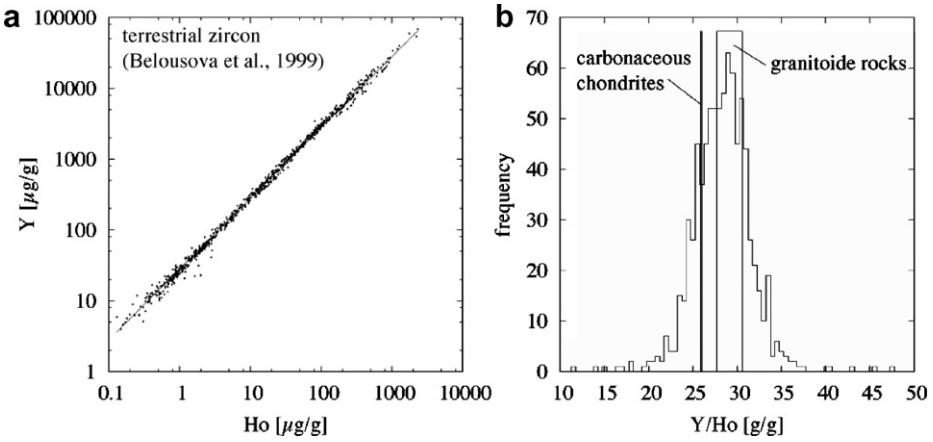

Fig. 8. (a) Plot of Y vs. Ho of 839 zircon LA-ICPMS analyses from different igneous rock types (Belousova et al., 2002; tabulated analyses were made available by E. A. Belousova). For comparison, the carbonaceous chondrite-defined Y/Ho-ratios are shown. (b) Histogram showing the distribution of the Y/Ho-ratios in zircons from igneous rocks. The carbonaceous chondrite-defined and the Y/Ho-ratio of felsic rocks are displayed.

Based on available analyses of rock standards, Bau (1996) arbitrarily defined a CHARAC field that ranges from Y/Ho ~24–36 and includes 83% of igneous rock geostandards with <70 wt.% SiO_2. Geostandards with SiO_2 exceeding 70 wt% showed systematically higher Y/Ho-ratios. The compilation of Y/Ho-ratios from the database by Jochum et al. (2005) confirmed the limits of the CHARAC-range given by Bau (1996). He suggested that deviation from CHARAC-behavior, i.e., Y/Ho-fractionation is due to the complexation behavior of Y and Ho in volatile-rich silica-rich melts. This implies that a highly evolved, volatile-rich magma behaves similar to an aqueous solution, for which Y/Ho-fractionation was experimentally demonstrated (Bau, 1999). Fractionation of Y and Ho, however, could also be due to differences in the non-ideality (activity coefficients) of Y and Ho components in silicate melts and be unrelated to the presence of volatile components. It was shown that the degree of melt polymerization has a strong effect on the ratio of the solubilities of $ZrSiO_4$ and $HfSiO_4$ in silicate melts (Linnen and Keppler, 2002). A similar mechanism could control the Y/Ho-ratio during formation of silica-rich melts (i.e., granites, rhyolites) and crystallization of zircon. If representative, our spinel lherzolite and basalt data support this view in that they show that fractionation of Y and Ho does occur during partial melting without presence of large quantities of water. We suggest that complexation of Y and Ho does not play a role in Y/Ho-fractionation, but that Y/Ho-fractionation is an anhydrous process that is related to the concentration SiO_2. If so, Y and Ho fractionation is expected to follow the same trends as Nb/Ta and Zr/Hf (Münker et al., 2003).

5.3.5. Y/Ho as tracer for the origin of the host rock of the Earth's earliest traces of life?

A highly metamorphosed quartz-pyroxene rock on the southwestern tip of Akilia Island has for long been the center of attention regarding the oldest traces of life on Earth. This five meter wide outcrop was originally interpreted as a Banded Iron Formation (BIF, Mojzsis et al., 1996; Nutman et al., 1997) and was found to contain graphite inclusions within apatite crystals (Mojzsis et al., 1996). The low $\delta^{13}C$ of these graphite inclusions suggested a biologic source material that had retained its original carbon isotope signature. Virtually every aspect of this claim has since been drawn into question; the age (Kamber and Moorbath, 1998; Whitehouse et al., 1999; Whitehouse and Kamber, 2005) and protolith (Fedo and Whitehouse, 2002a) of the rock itself, the age of the apatite crystals (Sano et al., 1999), and most recently the actual presence of graphite inclusions in apatite crystals (Lepland et al., 2005; Nutman and Friend, 2006). The debate on the protolith of this rock is a particularly contentious topic, since many different chemical and isotopic indicators for sedimentary and/or metasomatic processes appear to disagree with each other. This has led to two different views; the rock either represents a metamorphosed carbonate-rich BIF, or the rock represents a highly metasomatized ultramafic rock, which does not represent a marine depositional setting and would not be able to harbor traces of ancient life. The polarized state of the debate on this issue is clearly demonstrated by the recent, strongly contrasting studies of Manning et al. (2006) and Fedo et al. (2006). Both studies list the different chemical/isotopic indicators, and argue for or against a sedimentary origin respectively. Oxygen isotope systematics argue for a BIF origin (Manning et al., 2006), as do iron isotope systematics (Dauphas et al., 2004b). However, silicon isotope systematics argue against a sedimentary origin (Andre et al., 2006). Mass independent sulfur isotope anomalies have been used to argue for a sedimentary origin (Mojzsis et al., 2003), but a subsequent study failed to replicate these findings (Whitehouse et al., 2005). Particularly confusing are the different interpretations of immobile element ratios, and the chondrite- or PAAS-normalized REE patterns. Both types of indicators have been used to argue either for (Friend et al., 2002; Mojzsis and Harrison, 2002; Palin, 2002) or against (Bolhar et al., 2005; Fedo and Whitehouse, 2002a; Fedo and Whitehouse, 2002b; Fedo et al., 2006) a sedimentary origin. The observed Y/Ho ratio

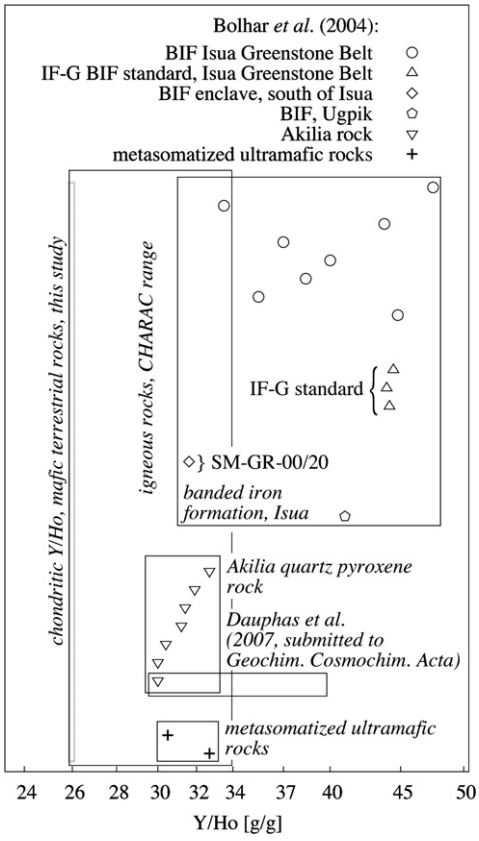

Fig. 9. Plot of Y/Ho of different Archean rocks from Greenland in comparison with our data from carbonaceous chondrites and terrestrial igneous rocks (data from Fedo and Whitehouse, 2002a; Bolhar et al., 2004) and Dauphas et al. (2007).

of ~31 (Fig. 9) falls within the CHARAC field as defined by Bau (1996) and is much lower than the values that are typically preserved in BIFs (Bau, 1999; Bau and Dulski, 1999). This would therefore argue for an igneous protolith. There are, however, several uncertainties that limit the use of the Y/Ho-ratio as a protolith indicator; the range of the CHARAC field, the range of Y/Ho-ratios encountered in igneous rocks, the effects of metasomatism. It is therefore important to further study the behavior of Y and Ho, and their potential use as an indicator for sedimentary protoliths in highly metamorphosed early Archean supracrustals.

6. SUMMARY AND CONCLUSIONS

Aerodynamic levitation melting in combination with LA-ICPMS is a suitable method for obtaining high-precision Y and Ho concentration data of bulk rocks. Our data show that there is not a uniform chondritic Y/Ho-ratio. Carbonaceous chondrites have a common Y/Ho-ratio of 25.94 ± 0.08 (2σ). This value is suggested to be the solar system Y/Ho-ratio. Systematically higher Y/Ho-ratios are observed in ordinary (LL: 26.06 ± 0.06, 2σ; L + H: 26.28 ± 0.05, 2σ) and enstatite (EL6: 27.25 ± 0.14, 2σ) chondrites. The origin of the fractionation is related to fractional condensation processes and loss of a refractory component from the region where the ordinary and EL6 chondrites formed. The relation between elevated Y/Ho and Re/Os in enstatite chondrites suggests that Re/Os-fractionation is also result of volatility-controlled nebular fractionation and that Re is more refractory than Os. It is not likely that the fractionation has been inherited from heterogeneous ISM dust. Within analytical uncertainty, chondrules from ordinary and CV3 chondrites do have a common Y/Ho-ratio of 26.22 ± 0.40. This indicates that small-scaled variations in Y/Ho did not exceed the few percent level. Differences in volatility of Y and Ho are shown on the basis of data from CAIs. The fractionation of Y and Ho is related to REE-fractionation. Ultrarefractory CAIs have supersolar Y/Ho, whereas CAIs with Group-II REE patterns have subsolar Y/Ho. This suggests that Y is more refractory than Ho. Data of a limited set of mafic terrestrial rocks indicate that the BSE has solar Y/Ho. A relation of the Earth and carbonaceous chondrites is consistent with our data, whereas formation of the Earth from enstatite chondrites is excluded. Y behaves more incompatibly during partial melting than Ho. This results in increasing Y/Ho from mafic to felsic rocks. Terrestrial zircons reflect the elevated Y/Ho-ratio of silica-rich igneous crustal rocks. The Y/Ho-fractionation is likely to be related to the properties of the melt and operates also in dry systems (i.e., partial mantle melting). Behavior Y and Ho in fluid-rich magmas similar to their behavior in aqueous solutions is not required. From our perspective, published Y/Ho-ratios in putative >3.85 Ga old quartz-pyroxene rock from the island of Akilia cannot be used as evidence for or against a sedimentary origin of these rocks.

ACKNOWLEDGMENT

J. Zipfel (Max-Planck-Institute Mainz), A. Bischoff (University of Münster), and R. Schumacher (University of Bonn) are thanked for loaning thin sections. B. Zanda (MHN Paris) provided material of Orgueil. H. St. C. O'Neill and D. Kelly are thanked for their support during the stay of AP at the RSES in Canberra. A. El Goresy (University of Bayreuth) kindly made available a spreadsheet with data from an ultrarefractory CAI. Inspiring discussions with R. Linnen and F. Holtz (Hannover) led to considerable improvements of the concepts regarding sources for Y/Ho-fractionations. R. Schönberg (Hannover) provided lherzolite material. AP gratefully acknowledges discussions with H. Palme (University of Cologne) and his support during this project. Constructive reviews by two anonymous referees, C. Floss and the AE helped to improve this manuscript.

This work benefited from funding by the German Science Foundation (DFG) through Grants PA346/24-1 (Herbert Palme, Cologne), PA909/1-1 and PA909/2-1 (AP, DFG Emmy-Noether-Program).

REFERENCES

Alexander C. M. O. D. (1994) Trace element distributions within ordinary chondrite chondrules: implications for chondrule formation conditions and precursors. *Geochim. Cosmochim. Acta* **58**, 3451–3467.

Andre L., Cardinal D., Alleman L. Y. and Moorbath S. (2006) Silicon isotopes in 3.8 Ga West Greenland rocks as clues to the

Eoarchaean supracrustal Si cycle. *Earth Planet. Sci. Lttrs.* **245**, 162–173.

Bau M. (1996) Controls on the fractionation of isovalent trace elements in magmatic and aqueous systems: evidence from Y/Ho, Zr/Hf, and lanthanide tetrad effect. *Contrib. Mineral. Petrol.* **123**, 323–333.

Bau M. (1999) Scavenging of dissolved yttrium and rare earths by precipitating iron oxyhydroxide: experimental evidence for Ce oxidation, Y-Ho fractionation, and lanthanide tetrad effect. *Geochim. Cosmochim. Acta* **63**, 67–77.

Bau M. and Dulski P. (1995) Comparative study of yttrium and rare earth element behaviors in fluorine-rich hydrothermal fluids. *Contrib. Mineral. Petrol.* **119**, 213–223.

Bau M. and Dulski P. (1999) Comparing yttrium and rare earths in hydrothermal fluids from the Mid-Atlantic Ridge: implications for Y and REE behavior during near-vent mixing and for the Y/Ho ratio of proterozoic seawater. *Chem. Geol.* **155**, 77–79.

Belousova E. A., Griffin W. L., O'Reilly S. Y. and Fisher N. I. (2002) Igneous zircon: trace element composition as an indicator of source rock type. *Contrib. Mineral. Petrol.* **143**, 602–622.

Bizzarro M., Baker J. A. and Haak H. (2004) Mg isotope evidence for contemporaneous formation of chondrules and refractory inclusions. *Nature* **431**, 275–278.

Blundy J. and Wood B. (2003) Partitioning of trace elements between crystals and melts. *Earth Planet. Sci. Lett.* **210**, 383–397.

Bolhar R., Kamber B. S., Moorbath S., Fedo C. M. and Whitehouse M. J. (2004) Characterization of early archean chemical sediments by trace element signatures. *Earth Planet. Sci. Lett.* **222**, 43–60.

Bolhar R., Kamber B. S., Moorbath S., Whitehouse M. J. and Collerson K. D. (2005) Chemical characterization of Earth's most ancient clastic metasediments from the Isua Greenstone Belt, southern West Greenland. *Geochim. Cosmochim. Acta* **69**, 1555–1573.

Boynton W. V. (1975) Fractionation in the solar nebula: condensation of yttrium and the rare earth elements. *Geochim. Cosmochim. Acta* **39**, 569–584.

Boynton W.V. (1989) Cosmochemistry of the rare earth elements: condensation and evaporation processes. In Rare Earth Elements (eds. B. R. Lipin and G. A. McKay). The Mineralogical Society of America, Washington. pp. 1–24.

Boynton W. V. and Frazier R. M. (1980) Identification of an ultrarefractory component in the Murchison meteorite. *Lunar Planet. Sci. Conf. XI*, 103–105.

Burris D. L., Pilachowski C. A., Armandroff T. E., Sneden C., Cowan J. J. and Roe H. (2000) Neutron-capture elements in the early galaxy: insights from a large sample of metal-poor giants. *Astrophys. J.* **544**, 302–319.

Byrne R. H. and Lee J. H. (1993) Comparative yttrium and rare earth element chemistries in seawater. *Mar. Chem.* **44**, 121–130.

Clayton R. N. (2004) Oxygen isotopes in meteorites. In *Meteorites, Comets, and Planets* (ed. A. E. Davis). Elsevier Pergamon, Amsterdam, pp. 129–142.

Dauphas N., Davis A. M., Marty B. and Reisberg L. (2004a) The cosmic molybdenum–ruthenium isotope correlation. *Earth Planet. Sci. Lett.* **226**, 465–475.

Dauphas N., van Zuilen M., Wadhwa M., Davis A. M., Marty B. and Janney P. E. (2004b) Clues from Fe isotope variations on the origin of early archean BIFs from Greenland. *Science* **306**, 2077–2080.

Dauphas, N., van Zuilen, M., Busigny, V., Lepland, A., Wadhwa, M., and Janney, P.E., 2007. Iron isotope, major and trace element characterization of early Archean supracrustal rocks from SW Greenland: protolith identification and metamorphic overprint. *Geochim. Cosmochim. Acta*, in press., doi:10.1016/j.gca.2007.07.019.

Davis A. M. and Grossman L. (1979) Condensation and fractionation of rare-earths in the solar nebula. *Geochim. Cosmochim. Acta* **43**, 1611–1632.

Dulski P. (2001) Reference materials for geochemical studies: new analytical data by ICP-MS and critical discussion of reference values. *Geostandard. Newsl. J. Geostandard. Geoanal.* **25**, 87–125.

El Goresy A., Zinner E., Matsunami S., Palme H., Spettel B., Lin Y. and Nazarov M. (2002) Efremovka 101.1: a CAI with ultrarefractory REE patterns and enormous enrichments of Sc, Zr, and Y in fassaite and perovskite. *Geochim. Cosmochim. Acta* **66**, 1459–1491.

Fedo C. M. and Whitehouse M. (2002a) Metasomatic origin of quartz-pyroxene rock, Akilia, Greenland, and implications for Earth's earliest life. *Science* **296**, 1448–1452.

Fedo C. M. and Whitehouse M. J. (2002b) Origin and significance of archean quartzose rock at Akilia, Greenland (reply). *Science* **298**, 917.

Fedo C. M., Whitehouse M. J. and Kamber B. S. (2006) Geological constraints in assessing the earliest life on Earth: a perspective from the Early Archean (>3.7 Ga) of southwest Greenland. *Philos. Trans. R. Soc. B* **361**, 851–867.

Fegley B. and Palme H. (1985) Evidence for oxidizing conditions in the solar nebula from Mo and W depletions in refractory inclusions in carbonaceous chondrites. *Earth Planet. Sci. Lett.* **72**, 311–325.

Freedman W. L., Madore B. F., Gibson B. K., Ferrarese L., Kelson D. D., Sakai S., Mould J. R., Kennicutt R. C., Ford H. C., Graham J. A., Huchra J. P., Hughes S. M. G., Illingworth G. D., Macri L. M. and Stetson P. B. (2001) Final results from the Hubble Space Telescope key project to measure the Hubble constant. *Astrophys. J.* **533**, 47–72.

Friend C. R. L., Nutman A. P. and Bennett V. C. (2002) Origin and significance of Archean quartzose rock at Akilia, Greenland (comment). *Science* **298**, 917.

Fröhlich C., Martinez-Pinedo G., Liebendörfer M., Thielemann F.-K., Bravo E., Hix W. R., Langanke K. and Zinner N. T. (2006) Neutrino-induced nucleosynthesis of A > 64 nuclei: the vp process. *Phys. Rev. Lett.* **96**, 142501.

Goldschmidt V. M., Barth T. and Lunde G. (1925) Geochemische Verteilungsgesetze der Elemente. V: Isomorphie und Polymorphie der Sesquioxide. Die Lanthaniden-Kontraktion und ihre Konsequenzen. *Skrifter utgit av Det Norske Videnskaps-Akademi i Oslo. I: Matem.-Naturvid. Klasse* **7**, 1–59.

Herndon J. M. (1996) Substructure of the inner core of the Earth. *Proc. Natl. Acad. Sci. USA* **93**, 646–648.

Hilton J. L. (1999) US Naval observatory ephemerides of the largest asteroids. *Astron. J.* **117**, 1077–1086.

Jarosewich E. (1990) Chemical analyses of meteorites: a compilation of stony and iron meteorites analyses. *Meteoritics* **25**, 323–337.

Javoy M. (1995) The integral enstatite chondrite model of the Earth. *Geophys. Res. Lett.* **22**, 2219–2222.

Jochum K. P., McDonough W. F., Palme H. and Spettel B. (1989) Compositional constraints on the continental lithospheric mantle from trace elements in spinel peridotite xenoliths. *Nature* **340**, 548–550.

Jochum K. P., Nohl U., Herwig K., Lammel E., Stoll B. and Hoffmann A. E. (2005) GeoReM: a new geochemical database for reference materials and isotopic standards. *Geostandard. Geoanal. Res.* **29**, 333–338.

Jochum K. P., Seifert H. M., Spettel B. and Palme H. (1986a) The solar-system abundances of Nb, Ta, and Y, and the relative abundances of refractory lithophile elements in differentiated planetary bodies. *Geochim. Cosmochim. Acta* **50**, 1173–1183.

Jochum K. P., Seufert H. M., Spettel B. and Palme H. (1986b) The solar-system abundances of Nb, Ta, and Y, and the relative abundances of refractory lithophile elements in differentiated planetary bodies. *Geochim. Cosmochim. Acta* **50**, 1173–1183.

Jones R. H. and Danielson L. R. (1997) A chondrule origin for dusty relict olivine in unequilibrated chondrites. *Meteorit. Planet. Sci.* **32**, 753–760.

Kamber B. S. and Moorbath S. (1998) Initial Pb of the Amitsoq gneiss revisited: implication for the timing of early Archean crustal evolution in West Greenland. *Chem. Geol.* **150**, 19–41.

Kornacki A. S. and Fegley, Jr., B. (1986) The abundance and relative volatility of refractory trace elements in Allende Ca,Al-rich inclusions: implications for chemical and physical processes in the solar nebula. *Earth Planet. Sci. Lett.* **79**, 217–234.

Lawler J. E., Sneden C. and Cowan J. J. (2004) Improved atomic data for Ho II and new holmium abundances for the Sun and three metal-poor stars. *Astrophys. J.* **604**, 850–860.

Lepland A., van Zuilen M. A., Arrhenius G., Whitehouse M. J. and Fedo C. M. (2005) Questioning the evidence for Earth's earliest life-Akilia revisited. *Geology* **33**, 77–79.

Linnen R. L. and Keppler H. (2002) Melt composition control for Zr/Hf fractionation in magmatic processes. *Geochim. Cosmochim. Acta* **66**, 3293–3301.

Lodders K. (2003) Solar system abundances and condensation temperatures of the elements. *Astrophys. J.* **591**, 1220–1247.

Longerich H. P., Jackson S. E. and Günther D. (1996) Laser ablation inductively coupled plasma mass spectrometry transient signal data acquisition and analyte concentration calculation. *J. Anal. Atom. Spectrom.* **11**, 899–904.

Manning C. E., Mojzsis S. J. and Harrison T. M. (2006) Geology, age and origin of supracrustal rocks at Akilia, West Greenland. *Am. J. Sci.* **306**, 303–366.

Mojzsis S. J., Arrhenius G., McKeegan K. D., Harrison T. M., Nutman A. P. and Friend C. R. L. (1996) Evidence for life on Earth before 3800 million years ago. *Nature* **384**, 55–59.

Mojzsis S. J. and Harrison T. M. (2002) Origin and significance of Archean quartzose rock at Akilia, Greenland (comment). *Science* **298**, 917.

Mojzsis S. J., Coath C. D., Greenwood J. P., McKeegan K. D. and Harrison T. M. (2003) Mass-independent isotope effects in Archean (2.5-3.8 Ga) sedimentary sulfides determined by ion microprobe multicollection. *Geochim. Cosmochim. Acta* **67**, 1635–1658.

Münker C., Pfänder J. A., Weyer S., Büchl A., Kleine T. and Mezger K. (2003) Evolution of planetary cores and the Earth–Moon system from Nb/Ta systematics. *Science* **301**, 84–87.

Nittler L. R. (2003) Presolar stardust in meteorites: recent advances and scientific frontiers. *Earth Planet. Sci. Lett.* **209**, 259–273.

Nordine P. C. and Atkins R. M. (1982) Aerodynamic levitation of laser-heated solids in gas jets. *Rev. Sci. Instrum.* **53**, 1456–1464.

Nozaki Y., Zhang Y. S. and Amakawa H. (1997) The fractionation between Y and Ho in the marine environment. *Earth Planet. Sci. Lett.* **148**, 329–340.

Nutman A. P. and Friend C. R. L. (2006) Petrography and geochemistry of apatites in banded iron formation, Akilia, W. Greenland: consequences for oldest life evidence. *Precambr. Res.* **147**, 100–106.

Nutman A. P., Mojzsis S. J. and Friend C. R. L. (1997) Recognition of >3850 Ma water-lain sediments in West Greenland and their significance for the early Archaean Earth. *Geochim. Cosmochim. Acta* **61**, 2475–2484.

Pack A., Shelley J. M. G. and Palme H. (2004a) Chondrules with peculiar REE patterns: implications for nebular condensation at high C/O. *Science* **303**, 997–1000.

Pack A., Shelley J. M. G. and Palme H. (2005) Origin of chondritic forsterite grains. *Geochim. Cosmochim. Acta* **69**, 3159–3182.

Pack A., Yurimoto H. and Palme H. (2004b) Petrographic and oxygen-isotope study of refractory forsterites from R-chondrite Dar al Gani 013 (R3.5-6), unequilibrated ordinary and carbonaceous chondrites. *Geochim. Cosmochim. Acta* **68**, 1135–1157.

Palme H. (2001) Chemical and isotopic heterogeneity in protosolar matter. *Philos. Trans. R. Soc. A* **359**, 2061–2075.

Palme H. and Jones A. (2004) Solar system abundances of the elements. In *Meteorites, Comets, and Planets* (ed. A. E. Davis). Elsevier, pp. 41–61.

Palme H. and Nickel K. G. (1985) Ca/Al ratio and the composition of the Earth's upper mantle. *Geochim. Cosmochim. Acta* **49**, 2123–2132.

Palme H. and Wlotzka F. (1976) Metal-particle from a Ca,Al-Rich inclusion from meteorite Allende, and condensation of refractory siderophile elements. *Earth Planet. Sci. Lett.* **33**, 45–60.

Palin J. M. (2002) The origin of a most contentious rock. *Science* **298**, 961.

Pearce N. J. G., Perkins W. T., Westgate J. A., Gorton M. P., Jackson S. E., Neal C. R. and Chenery S. P. (1997) A compilation of new and published major and trace element data for NIST SRM 610 and NIST SRM 612 glass reference materials. *Geostandard. Newsl.* **21**, 115–144.

Sano Y., Terada K., Takahashi Y. and Nutman A. P. (1999) Origin of life from apatite dating? *Nature* **400**, 127.

Schoenberg R. and von Blanckenburg F. (2006) Modes of planetary-scale Fe fractionation. *Earth Planet. Sci. Lett.* **252**, 342–359.

Shannon R. D. (1976) Revised effective ionic radii and systematics of interatomic distances in halides and chalcogenides. *Acta Crystallogr. A* **32**, 751–767.

Trinquier A., Birck J.-L. and Allègre C. J. (2007) Widespread ^{54}Cr heterogeneity in the inner solar system. *Astrophys. J.* **655**, 1179–1185.

Walker R. J., Horan M. F., Morgan J. W., Becker H., Grossman J. N. and Rubin A. E. (2002) Comparative ^{187}Re–^{187}Os systematics of chondrites: implications regarding early solar system processes. *Geochim. Cosmochim. Acta* **66**, 4187–4201.

Whitehouse M., Kamber B. S. and Moorbath S. (1999) Age significance of ion-microprobe U–Th–Pb zircon data from early Archaean rocks of West Greenland - a reassessment based on new combined ion-microprobe and imaging studies. *Chem. Geol.* **160**, 204–221.

Whitehouse M. J. and Kamber B. S. (2005) Assigning dates to thin gneissic veins in high-grade metamorphic terranes: a cautionary tale from Akilia, southwest Greenland. *J. Petrol.* **46**, 291–318.

Whitehouse M. J., Kamber B. S., Fedo C. M. and Lepland A. (2005) Integrated Pb- and S-isotope investigation of sulphide minerals from the early Archaean of southwest Greenland. *Chem. Geol.* **222**, 112–131.

Zhang J., Amakawa H. and Nozaki Y. (1994) The comparative behaviors of yttrium and lanthanides in the seawater of the North Pacific. *Geophys. Res. Lett.* **21**, 2677–2680.

Zhu X. K., Guo Y., O'Nions R. K., Young E. D. and Ash R. D. (2001) Isotopic homogeneity of iron in the early solar nebula. *Nature* **412**, 311–313.

Associate editor: Alexander N. Krot